Linearisation Method of DML-based Transmitters for Optical Communications Part III: Pulse Amplitude Modulation

N. Bamiedakis, D. G. Cunningham, *Member, IEEE*, and R.V. Penty, *Senior Member, IEEE*

***Abstract*— A new linearization method for optical transmitters based on directly modulated lasers (DMLs), named the Stretched A method, was proposed in Parts I and II of this work. Parts I and II presented the theoretical framework of the method for non-return-to-zero (NRZ) modulation and related detailed simulation and experimental results. Here, we extend the method to pulse amplitude modulation schemes (PAM). Focussing on 4-level PAM (PAM-4), we present the theoretical background and discuss implementations options. A simplified variation of the method for the generation of PAM signals with a significantly lower number of sub-currents is proposed. Simulation studies for PAM-4 transmission at 50 GBaud (100 Gb/s) and an experimental proof-of–principle demonstration at 16 GBaud (32 Gb/s) are reported based on 850 nm vertical-cavity surface-emitting lasers (VCSELs). For PAM-4, products of effective eye diagram areas (*PS*) of 0.6×10^{-5} and 43×10^{-5} before and after applying the Stretched A method were measured, demonstrating an improvement ratio of ~72. The sensitivity and tolerances of the method are analyzed using simulation and experiment.**

***Index Terms*— directly-modulated lasers, non-linearity, linearization method, optical transmitters, vertical-cavity surface-emitting lasers, pulse amplitude modulation**

I. Introduction

Short-reach optical communication links primarily employ transmitters based on directly-modulated lasers (DMLs) owing to their low cost and ease of implementation. However, their high-data-rate performance is limited by the non-linear behaviour of the DMLs when operated at high symbol rates. The laser non-linearity introduces significant distortion to the output optical waveform, which cannot be mitigated with conventional linear equalization methods. In order to address this issue, additional provisions must be made in the link optical power budget to account for the associated power penalties rendering the implementation of optical links at high symbol rates challenging. Different types of non-linear equalizers and equalization methods have been proposed and demonstrated to correct the laser non-linearity. These include asymmetric feedforward equalizers (FFE) [1-6], Volterra series equalizers [7-10], look-up tables [11-14] and machine-learning algorithms [15-18]. However, these methods are complex, power-hungry and rely on digital signal processing (DSP) either at the transmitter or the receiver. As a result, they have limited potential for use in low-cost, power-efficient optical links.

We have developed a new linearization method of optical transmitters based on DMLs, named the "Stretched A" (StrA) method, which can be easily implemented in practice [19, 20]. The method generates a modulating current waveform that approximates the ideal modulating current that produces a linear optical output waveform [14]. The method efficiently corrects most of the laser non-linearity while featuring large tolerances. In Parts I [19] and II [20] of this work, we presented its theoretical background. We reported detailed simulation and experimental studies on its use in an optical link using a vertical-cavity surface-emitting laser (VCSEL) and non-return-to-zero (NRZ) modulation. Here, we present the extension of the method to pulse amplitude modulation (PAM) schemes focussing primarily on 4-level PAM due to its great interest for use in real systems. We describe the implementation of the method and discuss possible variations which feature a more straightforward implementation. The performance achieved is studied via simulations and experiments on a VCSEL-based optical link. The results indicate that the application of the Stretched A method in its different variations enables the generation of 100 Gb/s (50 GBaud) PAM-4 optical waveforms with significantly reduced non-linearity using a vertical-cavity surface-emitting laser (VCSEL) with a 3dB bandwidth of 22 GHz. In addition, a proof-of-principle experimental demonstration of the Stretched method is reported using a 7 GHz 850 nm VCSEL. At 32 Gb/s (16 GBaud), conventional PAM-4 modulation exhibits closed PAM-4 eye diagrams. However, open PAM-4 eye diagrams with good linearity are achieved using the proposed simplified variation of the method. Furthermore, after passing the measured output PAM-4 optical waveforms through an FFE with 11 T-spaced taps, the conventional PAM-4 displayed small eye openings compared to the proposed simplified variation of the method. The ratio of the product of effective eye diagram areas (*PS*) metrics is shown to be ~72. The sensitivity and tolerances to parameter mismatch are also analyzed.

Manuscript received July xx, 2021; revised August xx, 2021; accepted September xx, 2021. Date of publication December xx 2021; date of current version November xx, 2021.

The authors would like to acknowledge the UK EPSRC for their support through the TOWS research grant (EP/S016570/1). Data related to this publication is available at the University of Cambridge data repository https://doi.org/10.17863/CAM.75097.

N. Bamiedakis, D.G. Cunningham and R. V. Penty are with the Centre for Photonic Systems, Electrical Engineering Division, Department of Engineering, University of Cambridge, Cambridge, CB3 0FA, UK.

(e-mail: nb301@cam.ac.uk). Digital Object Identifier xxxx

The remainder of the paper is structured as follows. Section II briefly reviews the Stretched A method and describes its application for PAM schemes. Section III presents simulation studies and its different variations while Section IV reports the proof-of-principle experimental demonstration. Finally, section V provides conclusions.

II. Stretched A method And PAM implementation

A. Basic theory

The ideal modulating current $I_{bc}(t)$ that produces a linear output optical waveform from a directly-modulated laser can be back-calculated from the standard laser rate equations [14]. The back-calculated current can be expressed as the sum of four sub-currents, named I_A, I_B, I_C and I_D which are related to the laser parameters, the photon density $N_p(t)$ in the laser cavity and its first and second order derivatives $N_p'(t)$ and $N_p''(t)$ respectively:

$$I_{bc}(t) = I_A(t) + I_B(t) + I_C(t) + I_D \quad (1)$$

The I_A sub-current contains the non-linear terms and terms with the second-order derivative N_p''. The I_B sub-current includes the terms proportional to the first-order derivative N_p'. The I_C sub-current comprises the terms which are proportional to the photon density N_p. The constant terms of the expression are grouped in the I_D sub-current. The exact expressions that define each sub-current were presented in Part I [19].

The photon density $N_p(t)$ in the laser cavity is proportional to the output optical power $P(t)$. As a result, in order to achieve a particular optical output waveform $P(t)$, the required photon density $N_p(t)$ can be found and the four sub-currents can be calculated. If the sub-currents could be accurately generated to form the total ideal back-calculated current $I_{bc}(t)$ and were fed to the laser, then the output optical waveform would have the desired shape: the exact implementation of eq. (1) is named here the ABCD method. However, the ABCD method is inherently hard to implement in practice as the expressions that provide the I_A and I_B sub-currents include terms that cannot be easily generated. As a result, we have proposed a new linearization method, which we have named the "Stretched A" method, which generates an approximation of the ideal back-calculated current $I_{bc}(t)$. This is achieved by generating suitable approximations for the I_A and I_B sub-currents which we name I_A^{st} and $\widetilde{I_B}$ respectively. These sub-currents are obtained via three steps: (i) we omit the least significant terms in their expressions, (ii) we replace the $1/N_p$ term with the inverse of the average photon density $\overline{N_p}$, and (iii) we scale and time shift the resulting sub-currents. Using these simplifications, I_A^{st} and $\widetilde{I_B}$ can be readily derived from the linear sub-current I_c via simple operations: differentiation, gain and time shift. The method was described in detail in Part I [19] and possible hardware implementations were discussed in Part II [20].

The total approximate modulating current $\widetilde{I_{bc}}$ obtained through the "Stretched A" method can therefore be written in the form:

$$\widetilde{I_{bc}}(t) = I_A^{st}(t) + \widetilde{I_B}(t) + I_C(t) + I_D \quad (2)$$

with the expressions for the three time-dependent sub-currents being:

$$I_C(t) = c \cdot N_p(t) \quad (3)$$

$$\widetilde{I_B}(t) = b\,\frac{dI_C(t)}{dt} \quad (4)$$

$$I_A^{st}(t) = \gamma \cdot \widetilde{I_A}(t + dt) \quad (5)$$

where $\widetilde{I_A}(t)$ is given by the expression:

$$\widetilde{I_A}(t) = a \cdot b\,\frac{d^2 I_C(t)}{dt^2} \quad (6)$$

The parameters c and b are constants that depend only on the laser parameters, while the parameter a is a scaling factor that depends on both the laser parameters and the operating point. These can be found analytically using the equations provided in Part I [19]. It is assumed that the laser parameters are either known by design or can be estimated through measurements. The amplitude scaling factor γ and timing offset dt for the I_A^{st} sub-current enable a better approximation of the ideal sub-current I_A and can be found adaptively by comparing the output optical waveforms with the target waveform, or the ideal sub-current I_A with the I_A^{st} for the different values of the parameters. Through simulation and experimental studies, it was shown in Part I [19]and II [20] that the generation of both the I_A^{st} and $\widetilde{I_B}$ sub-currents has relatively large tolerances making this scheme viable for real-world systems. Finally, it should be noted that here, as in Parts I and II this work [19, 20], it is assumed that any distortion of the driving signals due to the linear electrical channel from the laser driver to the laser are either minimised by design or corrected by some method (see section II.A in [19]).

B. Step response and PAM implementation

For a desired impulse response $h(t)$ for the output optical waveform, the ABCD and "Stretched A" methods can be applied to find the required sub-currents and total modulating current waveform to generate a single 0→1 transition at the output for each method. This has been described in detail in Part I, section III [19]. Assuming that the '0' and '1' output levels in $P(t)$ correspond to photon densities N_{p0} and N_{p1} respectively and that the transition takes place at t_0, the required photon density $N_p(t)$ in the laser cavity to achieve the desired output step response takes the shape:

$$N_p^{0\to1}(t) = N_{p0} + \left(N_{p1} - N_{p0}\right) \cdot \int_{-\infty}^{t} h(t - t_0)dt \quad (7)$$

The three time-dependent sub-currents and I_A or I_A^{st}, I_B or $\widetilde{I_B}$ and I_C to generate the 0→1 transition in the output optical waveform with the desired shape can be calculated based on eq. (3) – (6). Symmetric expressions can be derived for the negative 1→0 transition and therefore, for an arbitrary data pattern, the total modulating current can be obtained by summing up the respective positive and negative step responses for all transitions in the data. An example was provided in Part I, section III.C [19].

The implementation of the method for a PAM-M scheme follows the same principle; however, in order to generate the total modulating current I_{bc} (ABCD method) or $\widetilde{I_{bc}}$ (Stretched

A method), all possible transitions between the M signal levels need to be considered. For each positive transition $i \to j$ for $j > i$, the respective set of sub-currents (I_A, I_B, I_C) for the ABCD method, or $(I_A^{st}, \widetilde{I_B}, I_C)$ for the Stretched A method, must be generated. The shape of the I_C component is essentially the same for all transitions (apart from an offset and a scaled amplitude), while the shape of the ideal I_A and I_B sub-currents of the ABCD method are different for each transition. For the Stretched A method, however, it can easily be shown that the $\widetilde{I_A}$ and $\widetilde{I_B}$ sub-currents have the same shape for all transitions, but different amplitude. The amplitude of $\widetilde{I_B}$ for a particular transition $i \to j$ depends only on the magnitude $\Delta_{ij} = N_{pj} - N_{pi}$ of the transition, where N_{pi} and N_{pj} denote the photon densities at levels i and j respectively. The amplitude of the respective $\widetilde{I_A}$ sub-current depends on Δ_{ij} and the mean photon density for each transition $\overline{N_p^{i\to j}} = \frac{N_{pj}+N_{pi}}{2}$ via the a parameter (see eq. (15) in Part I [19]). As the ideal sub-current I_A is different for each transition, different γ and dt parameters need to be used to generate the optimised sub-current I_A^{st} from the $\widetilde{I_A}$ sub-current for each transition [eq. (5)]. Once the optimised set $(I_A^{st}, \widetilde{I_B}, I_C)$ has been determined for each positive transition $i \to j$, as in the NRZ case, the sub-currents for the opposite transitions $j \to i$ with $j > i$, can be readily obtained [19]. As a result, in order to implement the full Stretched A method, the number of the required basic sub-currents K that need to be generated is $N_{tr} + 2$, where N_{tr} is the number of possible transitions in a PAM-M signal:

$$N_{tr} = \binom{M}{2} = \frac{M \cdot (M-1)}{2} \tag{8}$$

Hence, K scales as $N_{tr} \sim O(M^2)$. In practice, therefore, the implementation of the full Stretched A method becomes challenging for PAM orders M larger than four. Even for PAM-4, six I_A^{st} sub-currents are required, along with the scaled versions of the $\widetilde{I_B}$ and I_C for each transition.

In order to overcome this limitation, an alternative simplified version of the Stretched A method for the generation PAM-M signals is proposed here to render it more practical for real-world implementation. The simplified method involves the use of a smaller subset of sub-currents N, with $1 \le N \le N_{tr}$, to generate all transitions N_{tr}. This is achieved by assigning an amplitude-scaled version of the employed N I_A^{st} sub-currents to the $N_{tr} - N$ transitions whose respective sub-current I_A^{st} is not being used. To illustrate this, Table I presents an example of an assignment of N I_A^{st} sub-currents, with N = 1 and 3, to the 6 transitions possible in a PAM-4 signal. For example, for the case $N = 1$, the sub-current $I_A^{st}(0 \to 3)$ for the largest transition 0→3 is used to define the sub-current I_A^{st} for all other transitions.

The proposed modification to the Stretched A method reduces the number of sub-currents required to generate the total modulating current $\widetilde{I_{bc}}$ but results in larger residual non-linearity in the output optical waveform $P(t)$ due to the use of non-optimised versions of the sub-current I_A for a subset of transitions. Obviously, the smaller the value of N, the larger the residual non-linearity is expected to be. The simulation studies and experimental results presented in the following sections demonstrate that the Stretched A method generates high-quality PAM-4 waveforms and indicate the performance achievable with different number N of sub-currents. Of particular interest is the implementation of the Stretched A method with $N = 1$ as it renders the generation of PAM-4 signals with significantly reduced non-linearity of similar complexity to the generation of NRZ signals. In this case, in total, three additional gain stages to scale the three sub-currents $(I_A^{st}, \widetilde{I_B}, I_C)$, for the three possible amplitudes of the transition $(\Delta, \frac{2}{3}\Delta, \frac{1}{3}\Delta)$ and synchronisation circuits to align the sub-currents are required. The details of the hardware implementation are not discussed here, but simulation and experimental results of the application of this method are shown for a VCSEL in the sections that follow. For the simulation and experimental studies presented here, we choose a Gaussian impulse response $h(t)$ as the desired impulse response for the output optical waveform as this has been widely used for VCSEL-based short-reach optical links [19].

TABLE I
EXAMPLE OF AN ASSIGNMENT OF THE N I_A^{st} SUB-CURRENTS FOR PAM-4 SIGNAL GENERATION WITH THE STRETCHED A METHOD.

Transition $i \to j$	$I_A^{st}(i \to j)$		
	$N = 1$	$N = 3$	$N = 6$ **(full method)**
0 → 1	$\frac{1}{3} \cdot I_A^{st}(0 \to 3)$	$\frac{1}{2} \cdot I_A^{st}(0 \to 2)$	$I_A^{st}(0 \to 1)$
0 → 2	$\frac{2}{3} \cdot I_A^{st}(0 \to 3)$	$I_A^{st}(0 \to 2)$	$I_A^{st}(0 \to 2)$
0 → 3	$I_A^{st}(0 \to 3)$	$I_A^{st}(0 \to 3)$	$I_A^{st}(0 \to 3)$
1 → 2	$\frac{1}{3} \cdot I_A^{st}(0 \to 3)$	$\frac{1}{3} \cdot I_A^{st}(0 \to 3)$	$I_A^{st}(1 \to 2)$
1 → 3	$\frac{2}{3} \cdot I_A^{st}(0 \to 3)$	$I_A^{st}(1 \to 3)$	$I_A^{st}(1 \to 3)$
2 → 3	$\frac{1}{3} \cdot I_A^{st}(0 \to 3)$	$\frac{1}{2} \cdot I_A^{st}(1 \to 3)$	$I_A^{st}(2 \to 3)$

III. SIMULATION STUDIES AND STR A VARIATIONS

Simulation studies are carried out on the generation of PAM-4 signals with reduced non-linearity using the proposed Stretched A method. The studies are performed using the VCSEL model based on rate equations presented in Part I [19] and are focussed on 50 GBaud (100 Gb/s) transmission due to the current increased interest in achieving such data rates with VCSEL-based short-reach optical links. The VCSEL parameters used in the model were reported in Part I, section III [19]. The 3dB bandwidth of the studied VCSEL is ~22 GHz at the bias current of 5 mA. The symbol rate used is 50 GBaud (100 Gb/s data rate), while the desired pulse response is the "IEEE" pulse response with 10% to 90% step response time T_C of $0.75 \times T$ [19]. Two pseudo-random binary sequences of length 2^7-1 (PRBS-7) appropriately scaled and offset are used to generate the PAM-4 data pattern used in the simulation and experimental studies. The VCSEL is assumed to be biased at 4.95 mA and modulated with a peak-to-peak current of 4.1 mA. The values used are the same as those assumed in the simulation studies for NRZ transmission in Part I [19].

A. *Step response*

Initially, the ideal I_A sub-current required to generate the ideal output step response for each positive transition $i \rightarrow j$, $j > i$, in the PAM-4 signal is calculated and is shown in Fig. 1(a). The respective normalised waveforms are shown in Fig. 1(b) to demonstrate their differences in shape. The optimum parameters γ and dt of the approximate I_A^{st} sub-currents are found adaptively using the root mean square error (RMSE) of the generated output optical waveform $\tilde{P}(t)$ in comparison to the target optical waveform $P(t)$[19]. Their values are shown in TABLE II. In addition, their estimated values obtained by comparing I_A^{st} with the ideal I_A with a similar RMSE metric (see section V in Part I [19]) are also shown for comparison.

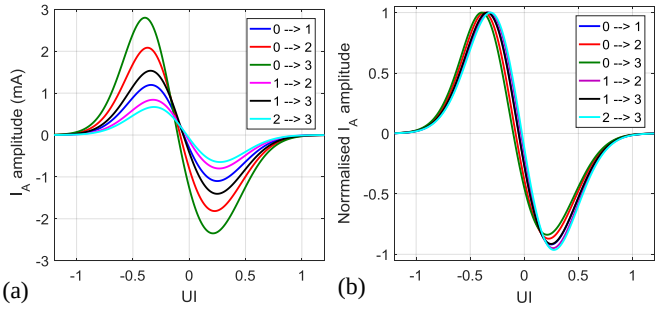

Fig. 1. (a) Ideal I_A sub-current to achieve the desired output step response for each positive transition in the PAM-4 signal and (b) normalised plots to show the differences in waveform shape (50 GBaud, $T_c = 0.75 \times T$).

TABLE II
OPTIMUM PARAMETERS FOR I_A^{st} FOR EACH POSITIVE PAM-4 TRANSITION WITH A RESOLUTION OF 0.01 FOR γ AND 0.005 UI FOR dt.

Transition $i \rightarrow j$	**Optical RMSE:** $\tilde{P}(t)$ vs $P(t)$		**Electrical RMSE** $I_A^{st}(t)$ vs $I_A(t)$	
	γ	dt **(UI)**	γ	dt **(UI)**
0 → 1	1.02	0.035	1.01	0.045
0 → 2	1.04	0.060	1.03	0.075
0 → 3	1.07	0.075	1.05	0.090
1 → 2	1.01	0.025	1.00	0.030
1 → 3	1.02	0.040	1.01	0.050
2 → 3	1.00	0.015	1.00	0.020

The slight difference in the optimum values of γ and dt obtained with the two methods is due to the fact that the electrical RMSE metric (I_A^{st} vs I_A) provides the parameters that yield the most similar waveform over its entire duration. However, the rising and falling edges of I_A^{st} appear to be more critical for generating an output optical waveform $\tilde{P}(t)$ as close as possible to the target waveform $P(t)$. This is exemplified in Fig. 2 where the ideal $I_A(t)$ sub-current for the 0→3 transition is compared with the optimum $I_A^{st}(t)$ obtained with the two metrics. However, the difference between the optimum values and the quality of the respective optical output waveforms is minimal [19], indicating that the electrical RMSE is a valuable metric that could provide near-optimum values for the γ and dt parameters without the need for optical simulations or measurements.

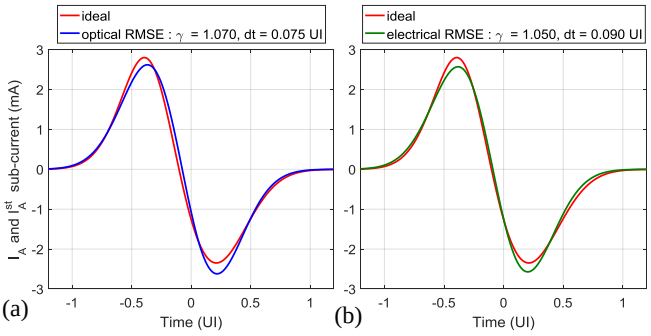

Fig. 2. Comparison of the ideal I_A with the estimated optimum I_A^{st} obtained through (a) the optical ($\tilde{P}$ vs P) and (b) the electrical RMSE (I_A^{st} vs I_A) metric for the 0→3 transition (50 GBaud, $T_c = 0.75 \times T$) .

B. *Full Stretched A method (N=6)*

The output optical PAM-4 waveform is obtained when the "full" Stretched A method ($N = 6$) is applied. Here, the optimum parameters γ and dt obtained for each step transition (TABLE II) are employed for the corresponding $I_A^{st}(t)$ sub-current. For comparison, the output optical waveforms for conventional PAM-4 modulation without any correction for non-linearity and the ideal ABCD method are also obtained for the same bias current and peak-to-peak modulation. The output PAM-4 optical waveforms are fed to an 11-tap T-spaced feedforward equalizer (FFE) to mitigate the linear distortions in the waveforms. The quality of the obtained waveforms is assessed by examining the respective PAM-4 eye diagrams and deriving metrics for each sub-eye i ($i = 1, 2, 3$): width (w_i), height (h_i) and effective area $S_i = w_i \times h_i$. In addition, the product PS of the effective areas S_i ($PS = \prod_{i=1}^{M-1} S_i$) is calculated and is also used to assess the quality of the PAM-4 eye diagrams. A PAM-4 eye diagram with more uniform sub-eyes would provide a larger PS metric than one with a similar sum of effective areas S_i but with greater imbalance between them. Finally, for the equalized waveforms, the noise enhancement factor (NEF) is also recorded. Fig. 3 shows the obtained eye diagrams of the output optical waveform before and after equalization for the different cases studied. It can be seen that the conventional PAM-4 modulation yields eye diagrams that are closed before equalization [Fig. 3(a)] and with very small eye openings after applying the 11-tap FFE [Fig. 3(d)]. On the other hand, the full Stretched A method ($N = 6$) corrects most of the laser non-linearity yielding open eye diagrams [Fig. 3(c) and Fig. 3(f)] which are very similar to the ones obtained with the ideal back-calculated current (ABCD method) [Fig. 3(b) and Fig. 3(e)]. Their respective eye diagram metrics are nearly identical, with any small differences observed attributed to the computational accuracy of the simulated waveforms and the derivation of the metrics from the output optical waveforms.

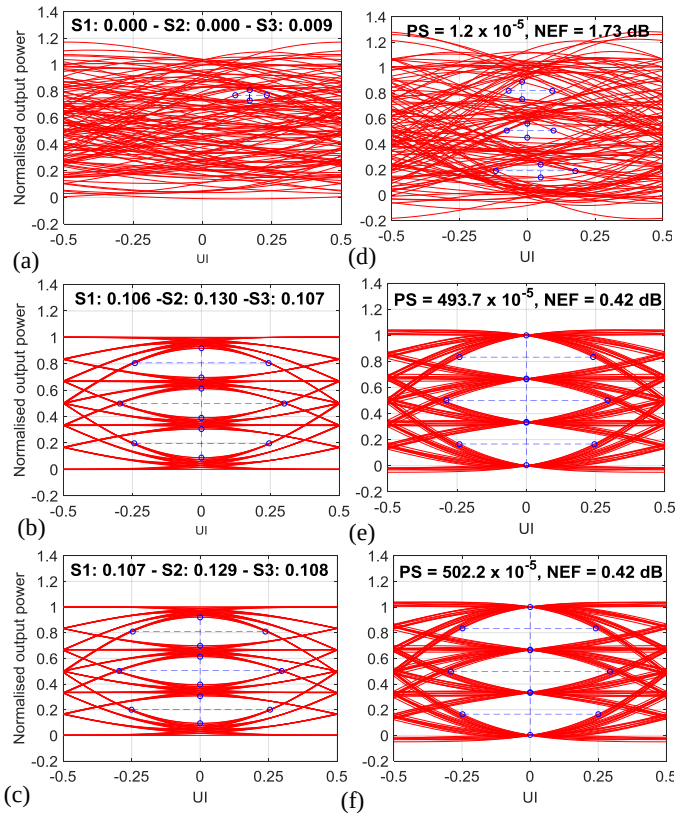

Fig. 3. Eye diagrams for 50 GBaud (100 Gb/s) PAM-4 transmission (a-c) before and (d-f) after the application of the 11-tap FFE equalizer (a and d) without any non-linear correction, (b and e) for the ideal back-calculated modulating current $I_{bc}(t)$, and (c and f) the approximated $\widetilde{I_{bc}}(t)$ using the full Stretched A method ($N = 6$). The desired step response time T_C is set to $0.75 \times T$.

C. *Simplified Stretched A method ($1 \leq N < 6$)*

As described previously, the proposed simplified variation of the Stretched A for the generation of PAM-M waveforms involves the use of a sub-set of N sub-currents out of the N_{tr} sub-currents of the full Stretched A method to generate the remaining $N_{tr} - N$ transitions in the modulating current waveform. Of particular interest is the use of a single sub-current set, denoted as the $N = 1$ variation. The selection of the γ_m and dt_m parameters (with $m = [1,..,N]$) for the employed N sub-currents affects the quality of the obtained waveforms. Different approaches can be used to optimise the values of the parameters using metrics based on either the ideal back-calculated modulating current waveform, the target PAM-M optical output waveform, or the respective waveforms for the individual NRZ transitions (TABLE II). We have developed a method described below that generates an optical PAM-M output waveform which is very close to that obtained with the ABCD and full Stretched A methods. This involves (i) scaling the employed I_A^{st} and $\widetilde{I_B}$ sub-current appropriately for each transition with a fixed term and (ii) finding the optimum γ_m and dt_m parameters using either the RMSE metric or PS metric of the generated PAM-M waveform.

The scaling factor of the $\widetilde{I_B}$ sub-current is identical to that employed in the full Stretched A method and is the ratio of the magnitude of the transition $i \to j$ ($\Delta_{i\to j}$) to that of the assigned $k \to l$ transition ($\Delta_{k\to l}$). The I_A^{st} sub-current is scaled by the same factor and, in addition, by the ratio of the a parameter of the transition ($a_{i\to j}$) to that of the assigned $k \to l$ transition ($a_{k\to l}$). The $\alpha_{i\to j}$ parameter for each transition $i \to j$ is given by the expression [19]:

$$a_{i\to j} = \left(\frac{1}{\overline{N_p^{i\to j}}} + \varepsilon\right) \cdot \chi \tag{9}$$

where $\overline{N_p^{i\to j}}$ is the mean photon density for the $i \to j$ transition, ε is the gain compression factor of the laser, and χ is a term that depends only on the laser parameters (see eq. (15) in [19]). As a result, the ratio $a_{i\to j}/a_{k\to l}$ is a constant term which depends on a single laser parameter (ε) and the operating conditions (laser bias and peak-to-peak modulation amplitude) and which can be pre-defined. TABLE III summarises the scaling factors used for the I_A^{st} and $\widetilde{I_B}$ sub-currents for each transition $i \to j$ in the PAM-M waveform assuming that the sub-current set of the $k \to l$ transition is used to generate all transitions of the PAM-M signal.

TABLE III
I_A^{st} AND $\widetilde{I_B}$ SUB-CURRENTS FOR THE SIMPLIFIED STRETCHED A VARIATION FOR THE GENERATION OF PAM-M WAVEFORMS

Transition	Full method	Simplified variation
$i \to j$	$I_A^{st}(i \to j)$	$\frac{a_{i\to j}}{a_{k\to l}} \cdot \frac{\Delta_{i\to j}}{\Delta_{k\to l}} \cdot I_A^{st}(k \to l)$
	$\widetilde{I_B}(i \to j) = \frac{\Delta_{i\to j}}{\Delta_{k\to l}} \cdot \widetilde{I_B}(k \to l)$	

The γ_m and dt_m parameters (with $m = [1,..,N]$) of the employed N sub-currents are optimised using either the RMSE of the generated optical PAM-M waveform compared to the target waveform or its PS metric after equalization with the FFE. The employed optimisation metric (RMSE or PS) is a function of $2{\times}N$ variables (N γ_m and dt_m parameters). As a result, for $N = 1$, this variation can be readily applied as only two parameters (the γ and dt of the single sub-current employed) need to be optimised. Hence, the implementation for PAM-M is of similar complexity to the application of the Stretched A for NRZ modulation [19, 20]. For $N > 1$ a multi-variate optimisation on the output waveform would need to be performed.

Here, we apply the proposed simplified method for $N = 1$ and PAM-4 modulation (TABLE III), as the use of a single sub-current set to generate all six transitions in the PAM-4 is of particular interest. The RMSE and PS metrics of the output optical waveform are obtained for 50 GBaud (100 Gb/s) transmission using the same simulation parameters as those used for the ABCD and full Stretched A in the previous section. Fig. 4 shows the contour plots of the two metrics for the generated PAM-4 optical waveform as a function of the γ and dt parameters of the single I_A^{st} sub-current used (that of the 0→3 transition). The white and green dots in the plots indicate the location of the minimum RMSE and maximum PS values respectively. It can be seen that the method achieves

very low RMSE values ≤ 0.03 for a wide range of parameters and achieves a maximum PS value of ~420 ×10^{-5} which is comparable to that obtained with the ABCD [Fig. 3(e)] and full stretched A methods [Fig. 3(f)] (~500 ×10^{-5} for both). It can also be noticed that the two metrics (RMSE and PS) yield slightly different optimum values for the two parameters. We consider the PS metric as being more reliable for the determination of the optimum γ and dt parameters as the RMSE metric does not directly assess the linearity of generated waveforms (i.e., whether these can be successfully equalized with a linear FFE). However, the difference in the PS metric is small between the two optimised sets: a PS value of ~390×10^{-5} is achieved for the parameter values that minimise the RMSE [Fig. 4(b)].

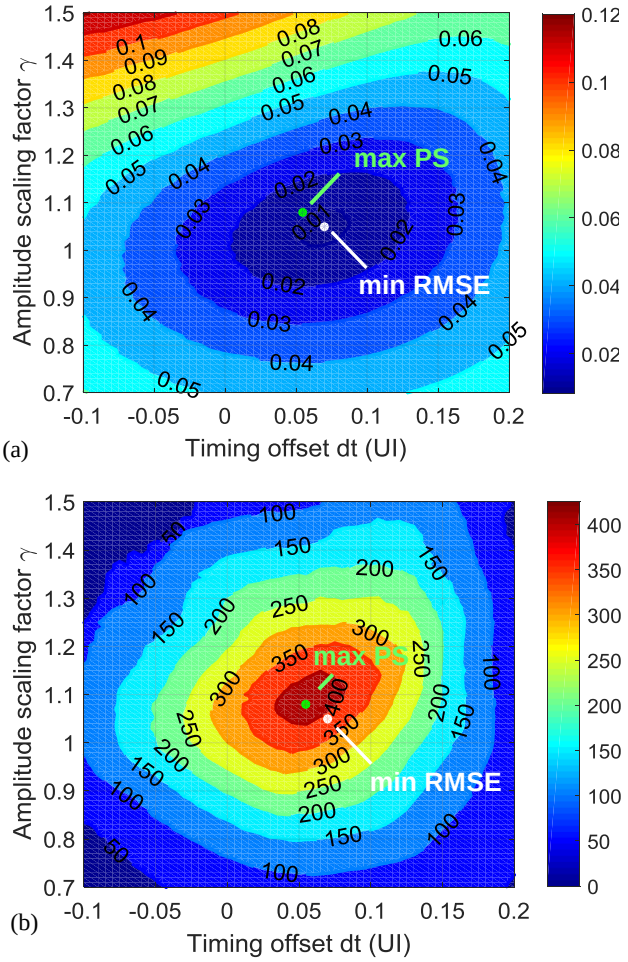

Fig. 4. (a) RMSE of the output PAM-4 optical waveform for 50 GBaud (100 Gb/s) transmission and (b) PS metric (×10^{-5}) after equalization with the T-spaced FFE as a function of the γ and dt parameters of the single sub-current $I_A^{st}(k \rightarrow l)$ used in the simplified Stretched A method ($N = 1$). The white and green dots indicate the location of the optimum parameter set for the RMSE and PS metric respectively: min RMSE: 0.008 for γ =1.05, dt=0.07 UI, max PS: 421×10^{-5} for γ =1.08, dt=0.055 UI.

The eye diagrams of the output PAM-4 optical waveform before and after equalization for the PS-optimised γ and dt parameters are shown in Fig. 5. The obtained eye diagrams are of very good quality and are very similar (as also demonstrated by their eye metrics) to those obtained from the full Stretched A method [(Fig. 3(c) and (f)] despite the significantly reduced number of sub-currents used.

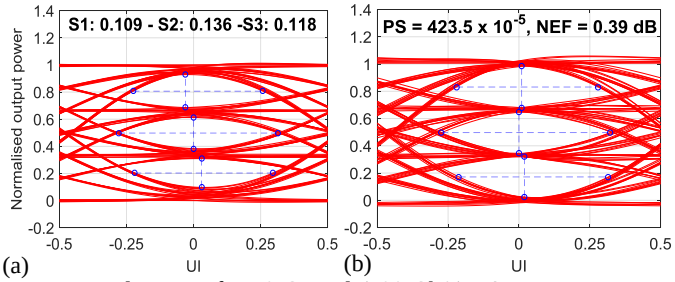

Fig. 5. Eye diagrams for 50 GBaud (100 Gb/s) PAM-4 transmission (a) before and (b) after equalization obtained with the simplified Stretched A method with $N = 1$ and the optimum parameters: γ = 1.08 and dt = 0.055 UI.

Fig. 4(b) also provides the sensitivity of the simplified $N = 1$ variation to the value of the γ and dt parameters of the employed I_A^{st}. It can be noticed that relatively large tolerances are obtained. For example, for achieving a PS metric ≥ 300×10^{-5}, a tolerance of approximately ±0.15 for γ and ± 0.06 UI for dt is achieved. Using a more relaxed specification of PS ≥ 200×10^{-5} provides larger tolerances of approximately ±0.18 for γ and ± 0.1 UI for dt. To associate these PS values with eye diagram quality, sample PAM-4 eye diagrams after equalization at 50 GBaud (100 Gb/s) obtained with the $N = 1$ variation and these specific values are shown in Fig. 6.

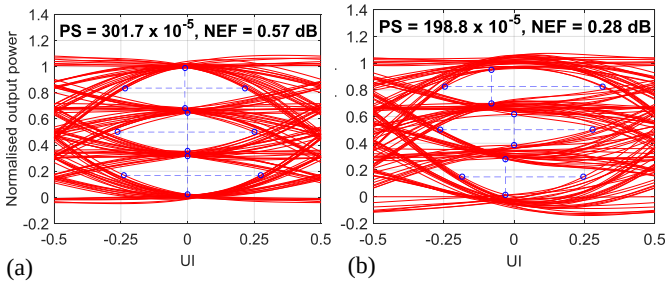

Fig. 6. Sample PAM-4 eye diagrams after equalization obtained at 50 GBaud (100 Gb/s) with the simplified Stretched A method with $N = 1$ with a PS metric of (a) ~300×10^{-5} (γ = 0.94 and dt = 0.045 UI) and (b) ~200×10^{-5} (γ = 1.37 and dt = 0.105 UI).

D. Tolerance to timing offset for $N = 1$ Stretched A variation

The tolerance of the $N = 1$ Stretched A variation to timing offsets in the alignment of the I_A^{st} component with the $\widetilde{I_B}$ and I_C sub-currents is investigated. A similar study has been performed for NRZ modulation in [19]. The introduced timing offset t_{off} shifts the positive and negative I_A^{st} pulses in the same direction with respect to their ideal timing (see Fig. 15 in [19]). For each timing offset, the total modulation current and the resulting output optical waveform are obtained with our rate equation model. The RMSE of the optical output waveform with respect to the target waveform and its PS metric after the application of the 11-tap FFE are calculated. Fig. 7 shows the obtained values and the respective eye diagrams for a selection of offsets. The non-ideal alignment of the sub-currents results in the degradation of the quality of the output optical waveform. The tolerance for achieving a PS value ≥ 300×10^{-5} is found to be approximately ±0.1 UI.

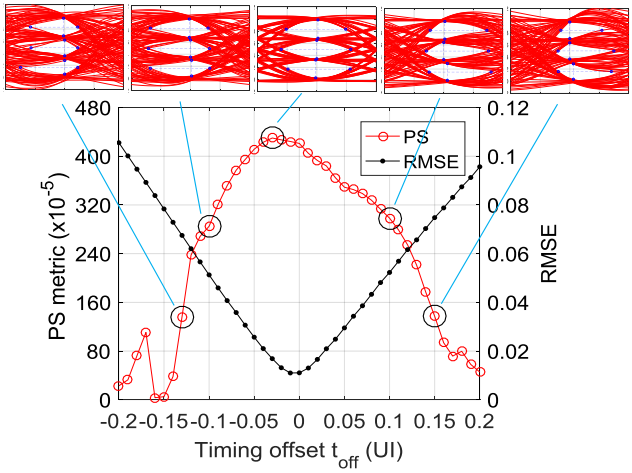

Fig. 7. RMSE of the output waveform and *PS* metric (×10^{-5}) of the eye diagram after equalization for the $N = 1$ Stretched A variation for 50 GBaud (100 Gb/s) PAM-4 transmission as a function on the timing offset t_{off}. The eye diagrams after equalization are also shown for a selection of offsets.

Similar to NRZ modulation [19], an adaptive gain scheme can also be applied for PAM-4 modulation to improve the tolerance to this timing offset. For each offset, the relative amplitude (scaling factors α and b) of the I_A^{st} and $\widetilde{I_B}$ sub-currents are adapted in order to improve the linearity of the output optical waveform. This is achieved by maximising the *PS* metric of the generated optical waveform after equalization. However, very similar results are obtained by minimising the RMSE metric. Fig. 8(a) shows the optimum values of the scaling factors, while Fig. 8(b) shows the values of the *PS* and RMSE metrics of the respective output optical waveform. The optimum scaling factors and plot behaviour are found to be very similar to those obtained for NRZ modulation [19]. The results demonstrate that the adaptive gain scheme provides significantly improved tolerance to this timing offset for the generation of PAM-4 signals through the simplified N = 1 Stretched A variation. The tolerance for achieving a *PS* value ≥ 300×10^{-5} is found to be approximately from -0.15 UI to 0.5 UI.

E. Discussion

Similar points can be raised regarding the implementation of the Stretched A method (full or simplified) for PAM-4 as the ones presented for NRZ modulation in [19] (see Section V). These are discussed briefly here with relevant simulation results provided.

(i) Choice of response time T_c: the choice of the step response time T_c affects the shape of the required sub-currents and the opening of the eye diagram of the optical output waveform before equalization. As a result, it dictates the bandwidth requirements of the driving electronics and the required performance of the linear equalizer to fully open the eye diagrams. A smaller T_c value requires larger bandwidth electronics but provides a larger eye opening and therefore requires a less powerful linear equalizer. A larger T_c value has the opposite effect. Fig. 9 shows the frequency spectrum of the I_A^{st} sub-current for T_c values of 0.6, 0.75 and $1.0 \times T$ while Fig. 10 shows the obtained eye diagrams at 50 GBaud (100

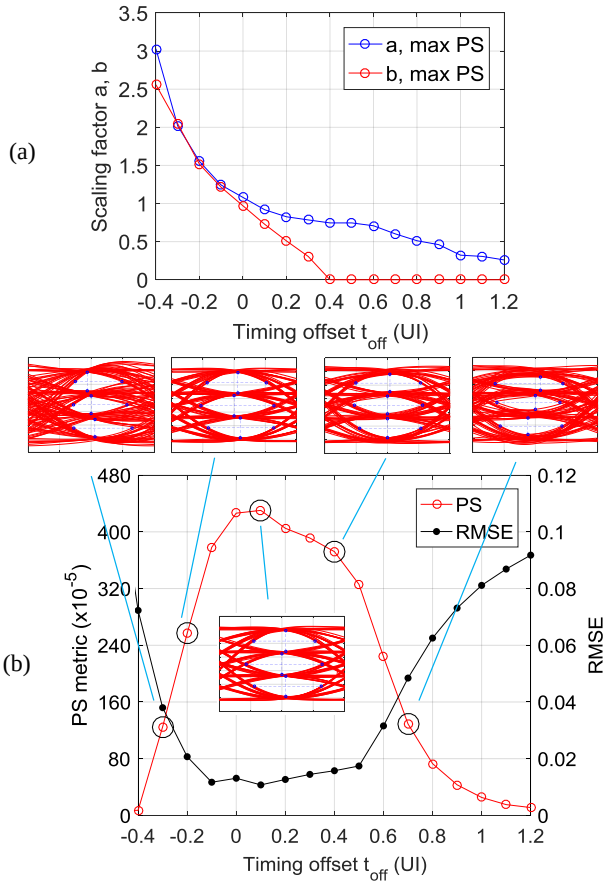

Fig. 8. (a) Scaling factors a and b for the adaptive gain scheme as a function of the timing offset t_{off} and (b) the corresponding *PS* metric and RMSE value of the generated output optical waveform. A selection of eye diagrams after equalization for different t_{off} values is also shown.

Gb/s) before and after equalization for T_c values of $0.6 \times T$ and $1.0 \times T$. Fully open eye diagrams are obtained in both cases after the application of the 11-tap T-spaced FFE. The smaller T_c value of $0.6 \times T$ results in a larger PS metric, mainly due to the larger eye width, and exhibits a very small NEF indicating very small values for the FFE tap coefficients. However, it imposes a more stringent bandwidth requirement on the driving electronics (Fig. 9).

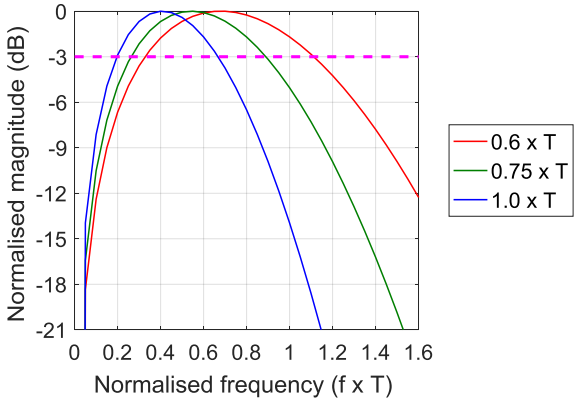

Fig. 9. Frequency spectrum of I_A^{st} sub-current for different values of the desired step response time T_c.

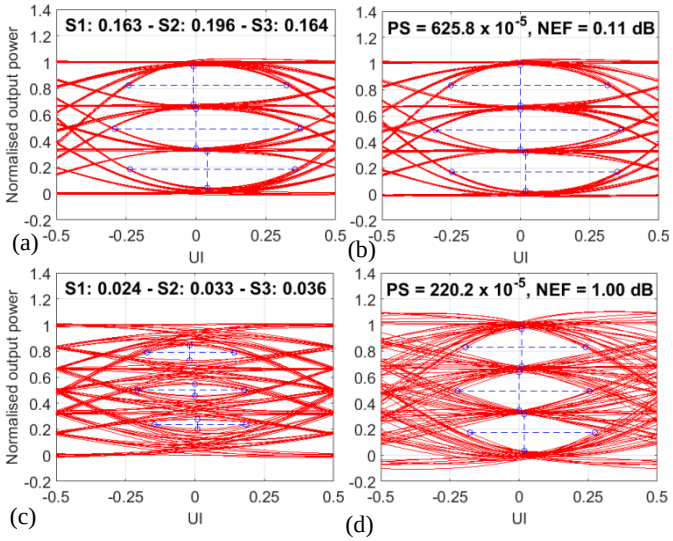

Fig. 10. 50 GBaud (100 Gb/s) PAM-4 eye diagrams (a and c) before and (b and d) after equalization obtained with the simplified Stretched A method with $N = 1$ for a step response time T_c of (a-b) $0.6 \times T$ and (c-d) $1.0 \times T$.

(ii) Pattern length: the Stretched A method works equally well for longer pattern lengths as it corrects the non-linearity in each transition. To exemplify this, Fig. 11 shows the simulated 50 GBaud (100 Gb/s) eye diagrams obtained for the transmission of PAM-4 data formed with PRBS-15 patterns for the full and simplified ($N = 1$) Stretched A method before and after equalization. The simulation parameters are the same as the ones used in the previous sections. Some performance degradation in comparison with the respective eye diagrams obtained for the PAM-4 pattern based on PRBS-7 is observed due to the residual non-linearity for the richer type of transitions in the transmitted data pattern. However, the quality of the obtained eye diagrams is very good, with most of the non-linearity corrected.

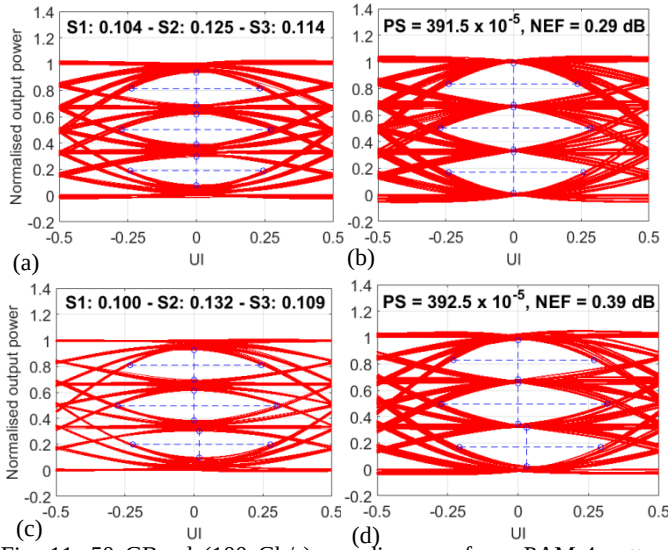

Fig. 11. 50 GBaud (100 Gb/s) eye diagrams for a PAM-4 pattern based on PRBS-15 (a and c) before and (b and d) after equalization obtained with (a-b) the full Stretched A method and (c-d) the simplified Stretched A method with $N = 1$.

IV. Proof-of-Principle Demonstration

A. Methodology and experimental setup

A commercially available 10 Gb/s 850 nm multimode VCSEL [21] is employed to demonstrate the proof-of-principle of the generation of PAM-4 signals with the Stretched A method. The simplified variation $N = 1$ is implemented here as the use of a single set of sub-currents to generate all transitions has the most significant potential for use in practice. The method is employed to generate 16 Gbaud (32 Gb/s) PAM-4 optical waveforms with a target 10% to 90% optical rise time T_c of $0.75 \times T$. The respective PAM-4 waveforms obtained for conventional modulation without any non-linear correction and for the full ABCD method are obtained for comparison. The lower data rate used in the experimental demonstration presented here compared to those presented in the simulation studies in the previous section (50 GBaud) is due to the equipment available. However, in both cases the employed symbol rate is roughly double the 3 dB laser bandwidth.

The VCSEL is mounted onto an SMA connector and wire bonded. The laser parameters are unknown, so the light-current characteristic and the small-signal frequency response are measured and employed to estimate these through a standard fitting process [20, 22-25]. Fig. 12 shows the measured light-current characteristic and 3 dB bandwidth as well as the simulated values using the rate equation model with the fitted parameters. A good fit is achieved. The small-signal 3 dB bandwidth of the VCSEL is found to be ~7 GHz for a ~5 mA bias current which is at the middle of the linear region of the device operation.

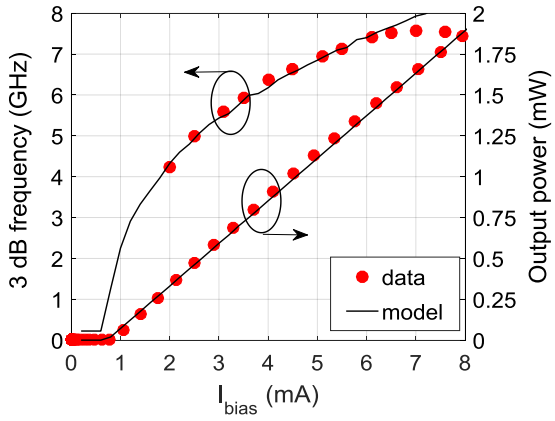

Fig. 12. Measured and simulated 3dB frequency and output optical power (coupled into a 50 µm MMF via a pair of microscope objectives) of the VCSEL as a function of the bias current.

The modulating current waveform for the ABCD and Stretched A method with $N = 1$ are obtained using the equations presented in Part I [19]. Once these are derived, linear pre-distortion is applied onto them to correct for the laser parasitics and ensure that the shape of modulating current reaching the actual laser is as close as possible to the desired one [20]. The modulating waveforms are appropriately sampled offline and generated with a 50 GS/s arbitrary waveform generator (AWG, Tektronix 70001A) with 14 GHz analog bandwidth. An oversampling ratio of 3 (48 GS/s) is employed for the 16 GBaud PAM-4 data transmission tests.

Fig. 13 shows the experimental setup used in the data transmission tests. The modulating current is generated by the AWG, amplified with a 40 GHz RF amplifier and fed to the VCSEL via a high-bandwidth bias tee. The VCSEL is biased at ~5.3 mA. The output light is coupled to a 50 μm MMF patchcord via a pair of microscope objectives (16× and 10×). The power level at the receiver is adjusted with a multimode variable optical attenuator (MM VOA). A 32 GHz optical sampling module (80C15) of a digital sampling oscilloscope (Tektronix DSA8300) is used as the optical receiver for the data transmission tests. The received optical power is set to +1 dBm for all data transmission tests. The eye diagram and the averaged trace of the received waveform are saved and offline processed. The offline processing includes the application of an 11-tap FFE to correct for linear distortions and the extraction of the metrics of each sub-eye for the PAM-4 eye diagrams before and after the application of the FFE: width w_i, height h_i and effective area $S_i = w_i \times h_i$. The PS metric (product of the S_i) after the application of the FFE is also calculated and is used to assess the linearity of the optical waveforms.

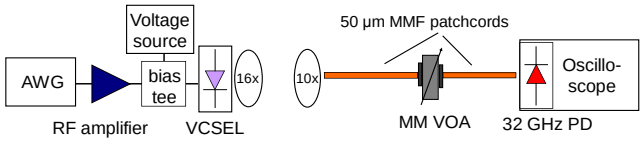

Fig. 13. Experimental setup for the data transmission experiments.

B. *Eye diagrams*

Fig. 14 shows the measured eye diagrams of the output optical waveforms before and after offline equalization with the 11-tap FFE for the three modulation currents: conventional PAM-4 without any non-linear correction [Fig. 14(a) and (d)], the ABCD method [Fig. 14(b) and (e)] and the $N = 1$ Stretched A variation [Fig. 14(c) and (f)]. For the offline equalization, the averaged (quasi noise-free) waveforms are employed to minimise the effect of noise on the optimisation of the FFE taps. As a result, the eye diagrams after equalization are quasi noise-free [Fig. 14(d-f)].

It can be clearly noticed that the conventional PAM-4 modulation without any non-linear correction results in a closed eye diagram. Some eye-opening is recovered after the application of the FFE but the equalized eye diagram exhibits significant skew, jitter, level thickness and overshoot due to the non-linearity of the generated output optical waveform. On the contrary, both the ABCD and the Stretched A ($N = 1$) methods correct for much of the non-linear distortions yielding open eye diagrams before and after equalization. The eye metrics obtained for the two methods are very similar, demonstrating that the simplified variation $N = 1$ of the Stretched A method successfully corrects most of the non-linear distortions of the optical waveform. The residual non-linearity is due to (i) the quality of the electrical signal generated by the AWG and (ii) the estimation of the VCSEL parameters through the small-signal measurements [20]. In order to assess the quality of the electrical signal generated by the AWG, its electrical output waveform is recoded for conventional NRZ modulation at 16 Gb/s after averaging. Fig. 15 shows the obtained noise-free eye diagrams before and after equalization at the receiver with the 11-tap FFE equalizer with the relevant metrics noted. It can be seen that these exhibit significant jitter and level thickness with an effective area S of ~0.8 after equalization. In contrast, in the simulations, the electrical modulating waveform is assumed to be ideal.

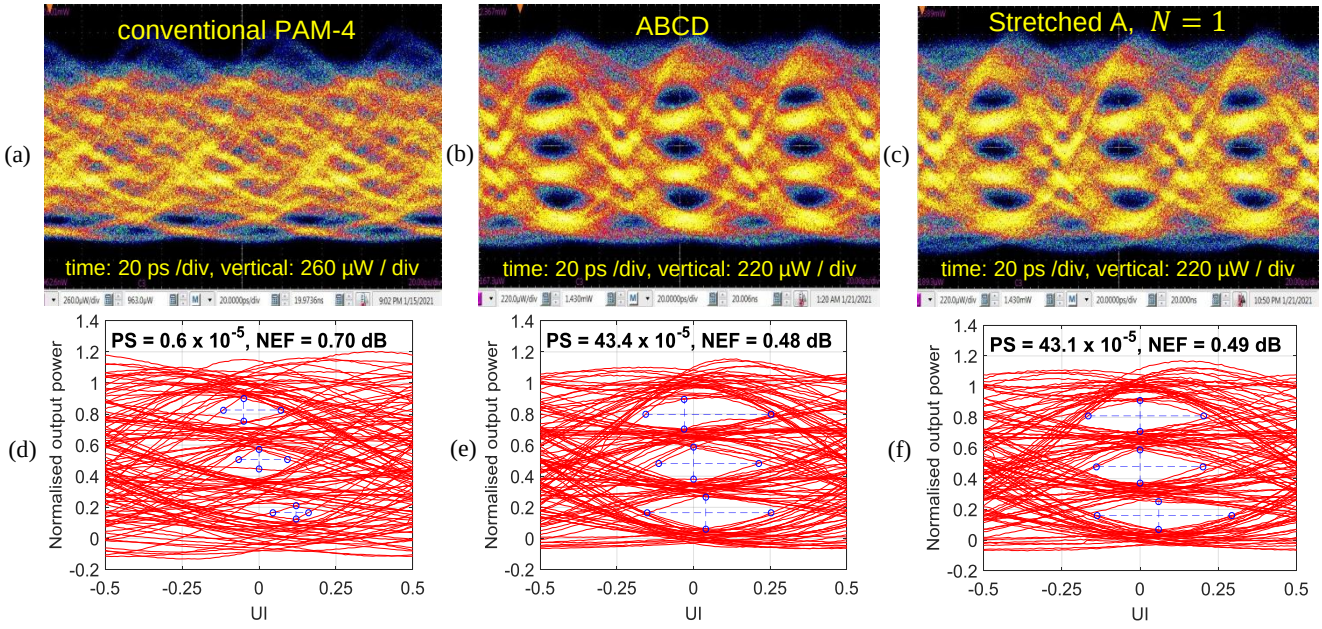

Fig. 14. Eye diagrams with metrics (a-c) before and (d-f) after offline equalization for (a and d) conventional modulation without any non-linear correction, (b and e) the ABCD method and (c and f) the $N = 1$ Stretched A variation for 16 GBaud (32 Gb/s) PAM-4 transmission.

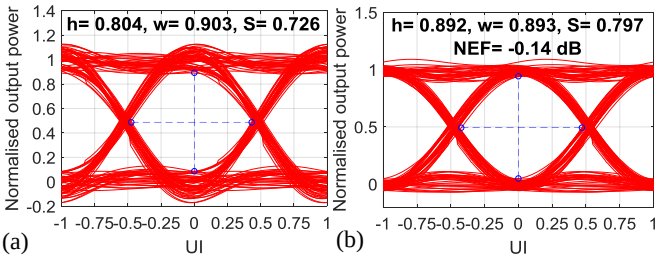

Fig. 15. Eye diagrams of the electrical output of the AWG (modulating electrical waveform) for conventional NRZ modulation at 16 Gb/s (a) before and (b) after equalization with the 11-tap FFE.

C. *Sensitivity analysis for parameters γ and dt*

The γ and dt parameters of the I_A^{st} sub-current used to generate all transitions are swept to find their optimum values and tolerances for the application of the $N = 1$ variation of the Stretched A method. For each set of parameters, the averaged output optical waveform is recorded, the 11 tap FFE is applied offline to mitigate the linear signal distortions and the *PS* metric of the eye diagram after equalization is calculated. Fig. 16(a) shows the obtained values normalised to the maximum value, which is found to be 45×10^{-5} for γ = 1.02 and dt = 0.04 UI. Its location is indicated in the contour plot with a green dot. Fig. 16(b) shows the normalised *PS* metric obtained through the simulations using the rate equation model and the fitted parameters. The location of the maximum point is found to be at γ = 1.06 and dt = 0.055 UI (green dot in plot) with a *PS* value of 408×10^{-5}. The contour plots exhibit similar shapes, while the positions of the optimum parameters are relatively close. The simulations yield much higher *PS* values as the VCSEL modulating current is assumed to be ideal. As indicated previously, the quality of the PAM-4 waveforms is limited by the quality of the electrical modulating signal generated by the AWG. Fig. 16(a) provides the tolerances of the Stretched A method for the generation of the I_A^{st} sub-current. The dashed line contour in the plot encloses the area which yields *PS* values which are ≥ 60% of the maximum value. The limits are roughly ±0.12 for γ (0.9 to 1.14) and -0.04 UI to +0.08 UI for dt (0.0 UI to 0.12 UI).

D. *Tolerance to timing offset*

The tolerance to the timing offset t_{off} in the alignment of the I_A^{st} with the $\widetilde{I_B}$ and I_C sub-currents is experimentally investigated for the $N = 1$ variation of the Stretched A method. The output optical waveform generated for different t_{off} is recorded and the *PS* metric is obtained after the offline application of the 11-tap FFE. The variation of the *PS* metric is shown in Fig. 17 (red line with circles). The tolerance to achieve a *PS* metric of ≥ 60% of the maximum value (here ~24×10^{-5}) is approximately ±0.05 UI. The adaptive gain scheme presented in section III.D is applied to improve this. Fig. 17 (blue line with squares) shows the obtained *PS* values after the application of the adaptive gain scheme. The tolerance to t_{off} has been increased by roughly 4 times, with t_{off} values in the range -0.15 to +0.25 UI yielding a *PS* value ≥ 24×10^{-5}. The small difference in the maximum *PS* values recorded at t_{off}=0.0 UI is due to the effect of noise in the recorded waveforms and experimental variations.

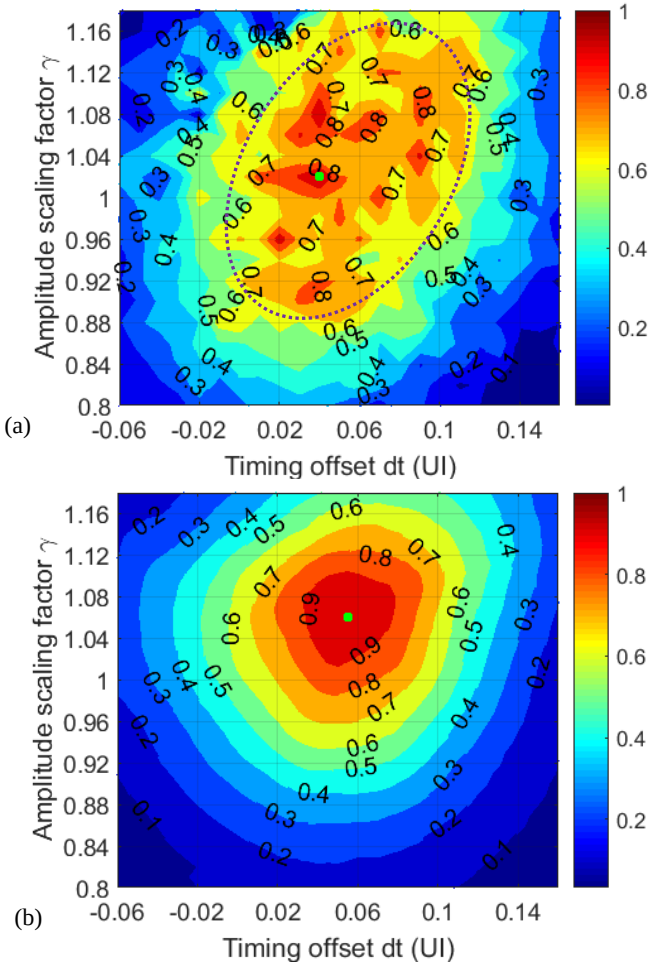

Fig. 16. (a) Experimental and (b) simulated *PS* metric normalised to its maximum value as a function of the γ and dt parameters of the Stretched A $N = 1$ variation. The green dot in the plots indicates the location of the maximum. Experiments: γ = 1.02, dt = 0.04 UI. Simulations: γ = 1.06, dt = 0.055 UI.

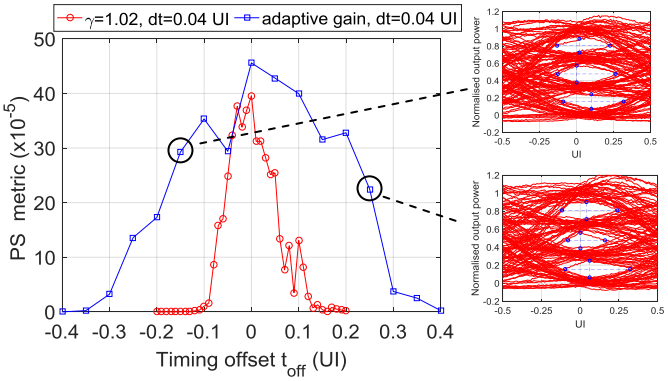

Fig. 17. *PS* metric of the PAM-4 eye diagrams after offline equalization as a function of the timing offset t_{off} with and without adaptive gain. The inset plots show the eye diagrams after equalization for t_{off}= -0.15 UI (top, *PS*=29×10^{-5}) and +0.25 UI (bottom, *PS*=22×10^{-5}).

V. Conclusions

The Stretched A method allows the generation of PAM-*M* optical waveforms with significantly reduced non-linearity.

Through simulation and experiment, it is shown here that it is possible to reduce the number of employed sub-current sets of the method, thereby significantly improving its practicability. Furthermore, a simplified variation of the method that uses a single sub-current set is proposed. This variation, named $N = 1$, can provide high-quality optical PAM-4 waveforms with significantly reduced non-linearity comparable to that achieved by the full ABCD method. The $N = 1$ variation is demonstrated experimentally using 7 GHz 850 nm VCSELs. Open 16 GBaud (32 Gb/s) PAM-4 eye diagrams are achieved and a 72× improvement in the PS metric over conventional PAM-4 modulation is demonstrated. It is also shown both via simulations and experiments, that the application of the method features relatively large tolerances and that the adaptive gain scheme can improve the tolerances to timing offsets in the alignment of the sub-currents.

REFERENCES

[1] G. Belfiore, M. Khafaji, R. Henker, and F. Ellinger, "A 50 Gb/s 190 mW Asymmetric 3-Tap FFE VCSEL Driver," *IEEE Journal of Solid-State Circuits*, vol. 52, pp. 2422-2429, 2017.

[2] K. Ohhata, H. Imamura, Y. Takeshita, K. Yamashita, H. Kanai, and N. Chujo, "Design of a 4 x 10 Gb/s VCSEL Driver Using Asymmetric Emphasis Technique in 90-nm CMOS for Optical Interconnection," *IEEE Transactions on Microwave Theory and Techniques*, vol. 58, pp. 1107-1115, 2010.

[3] A. S. Ramani, S. Nayak, and S. Shekhar, "A Differential Push-Pull Voltage Mode VCSEL Driver in 65-nm CMOS," *IEEE Transactions on Circuits and Systems I: Regular Papers*, vol. 66, pp. 4147-4157, 2019.

[4] M. Raj, M. Monge, and A. Emami, "A Modelling and Nonlinear Equalization Technique for a 20 Gb/s 0.77 pJ/b VCSEL Transmitter in 32 nm SOI CMOS," *IEEE Journal of Solid-State Circuits*, vol. 51, pp. 1734-1743, 2016.

[5] D. Liang, A. Roshan-Zamir, Y.-H. Fan, C. Zhang, B. Wang, A. Descos, W. Shen, K. Yu, C. Li, G. Fan, G. Kurczveil, Y. Hu, Z. Huang, M. Fiorentino, S. Kumar, S. M. Palermo, and R. G. Beausoleil, "Fully-Integrated Heterogeneous DML Transmitters for High-Performance Computing," *Journal of Lightwave Technology*, vol. 38, pp. 3322-3337, 2020.

[6] U. Hecht, N. Ledentsov, P. Scholz, M. Agustin, P. Schulz, N. N. Ledentsov, and F. Gerfers, "Non-Linear PAM-4 VCSEL Equalization and 22 nm SOI CMOS DAC for 112 Gbit/s Data Transmission," in *12th German Microwave Conference (GeMiC)*, 2019, pp. 115-118.

[7] Y. Yu, M. R. Choi, T. Bo, Z. He, Y. Che, and H. Kim, "Low-Complexity Second-Order Volterra Equalizer for DML-Based IM/DD Transmission System," *Journal of Lightwave Technology*, vol. 38, pp. 1735-1746, 2020.

[8] J. Liu, K. Chi, C. Wei, T. Lin, C. Chuang, X. Chen, J. Shi, and J. Chen, "High bit-rate distance product of 128 Gbps.km 4-PAM transmission over 2-km OM4 fiber using an 850-nm VCSEL and a Volterra nonlinear equalizer," in *Optical Fiber Communications Conference and Exhibition (OFC)*, 2017, pp. 1-3.

[9] N. Stojanovic, F. Karinou, Z. Qiang, and C. Prodaniuc, "Volterra and Wiener Equalizers for Short-Reach 100G PAM-4 Applications," *Journal of Lightwave Technology*, vol. 35, pp. 4583-4594, 2017.

[10] L. Ge, W. Zhang, C. Liang, and Z. He, "Threshold-Based Pruned Retraining Volterra Equalization for 100 Gbps/Lane and 100-m Optical Interconnects Based on VCSEL and MMF," *Journal of Lightwave Technology*, vol. 37, pp. 3222-3228, 2019.

[11] A. Tyagi, T. Iwai, K. Yu, B. Wang, W. Sorin, S. Mathai, M. Tan, and S. Palermo, "A 50 Gb/s PAM-4 VCSEL Transmitter With 2.5-Tap Nonlinear Equalization in 65-nm CMOS," *IEEE Photonics Technology Letters*, vol. 30, pp. 1246-1249, 2018.

[12] P. Gou, L. Zhao, K. Wang, W. Zhou, and J. Yu, "Nonlinear Look-Up Table Predistortion and Chromatic Dispersion Precompensation for IM/DD PAM-4 Transmission," *IEEE Photonics Journal*, vol. 9, pp. 1-7, 2017.

[13] A. S. Karar, M. YaÃ±ez, Y. Jiang, J. C. Cartledge, J. Harley, and K. Roberts, "Electronic dispersion pre-compensation for 10.709-Gb/s using a look-up table and a directly modulated laser," *Optics Express*, vol. 19, pp. B81-B89, 2011.

[14] A. S. Karar, J. C. Cartledge, J. Harley, and K. Roberts, "Electronic Pre-Compensation for a 10.7-Gb/s System Employing a Directly Modulated Laser," *Journal of Lightwave Technology*, vol. 29, pp. 2069-2076, 2011.

[15] S. Warm, C. Bunge, T. Wuth, and K. Petermann, "Electronic Dispersion Precompensation With a 10-Gb/s Directly Modulated Laser," *IEEE Photonics Technology Letters*, vol. 21, pp. 1090-1092, 2009.

[16] K. Burse, R. N. Yadav, and S. C. Shrivastava, "Channel Equalization Using Neural Networks: A Review," *IEEE Transactions on Systems, Man, and Cybernetics, Part C (Applications and Reviews)*, vol. 40, pp. 352-357, 2010.

[17] J. Estaran, R. Rios-Mueller, M. A. Mestre, F. Jorge, H. Mardoyan, A. Konczykowska, J. Dupuy, and S. Bigo, "Artificial Neural Networks for Linear and Non-Linear Impairment Mitigation in High-Baudrate IM/DD Systems," in *42nd European Conference on Optical Communication (ECOC)*, 2016, pp. 1-3.

[18] T. A. Eriksson, H. Bulow, and A. Leven, "Applying Neural Networks in Optical Communication Systems: Possible Pitfalls," *IEEE Photonics Technology Letters*, vol. 29, pp. 2091-2094, 2017.

[19] N. Bamiedakis, D. G. Cunningham, and R. V. Penty, "Linearisation Method of DML-based Transmitters for Optical Communications, Part I: Theory and Simulation Studies," in *IEEE Journal of Lightwave Technology*, Early Access, DOI: 10.1109/JLT.2021.3093517, 2021.

[20] N. Bamiedakis, D. G. Cunningham, and R. V. Penty, "Linearisation Method of DML-based Transmitters for Optical Communications, Part II: Experimental Demonstration and Implementation Methods," in *IEEE Journal of Lightwave Technology*, Early Access, DOI :10.1109/JLT.2021.3093845, 2021.

[21] Ulm Photonics (Philips) 10 Gbps 850 nm VCSEL chips, part ULM850-10-TN-N0101U.

[22] P. Westbergh, J. S. Gustavsson, B. Kogel, Ã. s. Haglund, and A. Larsson, "Impact of photon lifetime on high-speed VCSEL performance," *IEEE Journal of Selected Topics in Quantum Electronics*, vol. 17, pp. 1603-1613, 2011.

[23] S. W. Corzine, M. Mashanovitch, and L. A. Coldren, *Diode lasers and photonic integrated circuits*: Hoboken, New Jersey : Wiley, 2011.

[24] A. Larsson, "Advances in VCSELs for Communication and Sensing," *IEEE Journal of Selected Topics in Quantum Electronics*, vol. 17, pp. 1552-1567, 2011.

[25] S. B. Healy, E. P. O. Reilly, J. S. Gustavsson, P. Westbergh, H. Ã…, A. Larsson, and A. Joel, "Active Region Design for High-Speed 850-nm VCSELs," *IEEE Journal of Quantum Electronics*, vol. 46, pp. 506-512, 2010.